Nonlinear Least-Squares Post-Processing for Compressive Radar Imaging of A Rotating Target

Ngoc Hung Nguyen*, Kutluyıl Doğançay*, Hai-Tan Tran† and Paul Berry†
*School of Engineering, University of South Australia, Mawson Lakes, SA 5095, Australia
†National Security and ISR Division, Defence Science and Technology Group, Edinburgh, SA 5111, Australia

***Abstract*—In compressive radar imaging of rotating targets, conventional sparse reconstruction algorithms produce blurred and low-contrast reconstructed images of the target due to dictionary mismatch caused by off-grid scatterers. A nonlinear least-squares post-processing (NLSPP) method has recently been developed to tackle the blurring problem existing in the reconstructed images based on cluster analysis and nonlinear least-squares estimation (NLSE). In this paper, we propose a new improvement of the NLSPP method, which is called the I-NLSPP method, based on a reformulation of the NLSE process of the NLSPP method. Specifically, by jointly performing the NLSE process over all atom clusters using the original backscattered signal, the proposed I-NLSPP method results in more accurate estimates of the positions and reflectivities of the scatterers constituting the target. The superior performance of the proposed I-NLSPP method over the NLSPP method is demonstrated by way of simulation. In particular, we observe that the I-NLSPP method achieves a mean-squared-error performance much closer to the Cramér-Rao lower bound than the NLSPP method.**

I. Introduction

Radar imaging is fundamentally an inverse scattering problem with the objective of reconstructing a spatial map of reflectivity for a target of interest from limited measurements of scattered electromagnetic fields. In many radar imaging applications, the sparsity or compressibility of the reflectivity distribution of the target motivates the use of the emerging field of compressive sensing (CS) [1]–[11]. Examples of compressive radar imaging are found in coherence imaging [4], [5], wide-angle imaging of anisotropic scattering [7], radar imaging of target with rotating micro-motion [9]–[12], moving target indication [8], delay-Doppler radar imaging [3], and multi-channel imaging [6], to name but a few. In this paper, we focus on the problem of compressive radar imaging of a rotating target.

Radar imaging of rotating targets like propellers of a fixed-wing aircraft or rotor blades of a helicopter has recently attracted great attention in the literature [9]–[14]. The rotating motion of such targets belongs to the class of micro-motion which induces additional micro-Doppler frequency modulations in the scattered radar signal [13], [14]. The micro-Doppler modulations expose information about the target geometrical structure and thus can be exploited in the imaging process.

Early efforts to exploit the use of CS for radar imaging of rotating targets have been reported in [9]–[12]. The main principle behind these works is to construct a dictionary of signal prototypes (atoms) from a discrete parameter space, thus resulting in a linear relationship between the backscattered radar signal and the unknown reflectivity vector to be estimated. Since a typical target is composed of a small number of dominant scatterers, the reflectivity vector is sparse, i.e., containing a small number of nonzero elements, and the problem becomes finding a sparse solution of an under-determined linear inverse equation which can be effectively solved within the framework of CS. Unfortunately, the works in [9]–[12] are restricted to the on-grid scenario where the true scatterers constituting the target are assumed to be located exactly on the dictionary grid. In practice, the true scatterers are typically located off-grid. Such an off-grid problem causes conventional sparse reconstruction techniques to produce blurred and low-contrast images of the true target due to the position mismatch between the true scatterers and the dictionary grid nodes (see [15] and the references therein).

Recently, a nonlinear least-squares post-processing (NLSPP) method has been proposed in [15] to resolve the blurriness existing in the reconstructed images obtained via sparse reconstruction algorithms. Motivated by the observation that, in the reconstructed images, each off-grid scatterer typically induces a cluster of on-grid atoms in the surrounding vicinity of the scatterer due to the dictionary mismatch, the NLSPP method partitions the selected atoms given by the sparse reconstruction algorithm into a number of clusters and replaces the resulting clusters by equivalent scatterers with the positions and reflectivity coefficients computed from nonlinear least-squares estimation (NLSE). Since the NLSE process is performed in a continuous parameter domain, accurate estimates of the locations and reflectivities of the true off-grid scatterers are obtained. In consequence, the NLSPP method results in a sharp and intensity-correct image of the target.

A drawback of the NLSPP method [15] is that the NLSE procedure is performed individually for each cluster using the summed reconstructed signal of the atom members within the cluster. This reconstructed signal unfortunately is an imperfect approximation of the actual backscattered signal of the true scatterer associated with the cluster because of the mismatch between the positions of the true scatterers and dictionary grid nodes. Therefore, performing NLSE for each cluster individually limits the accuracy of the estimates of the positions and reflectivities of the true off-grid scatterers and thus the overall NLSPP performance.

The main contribution of this paper is to propose a new improved NLSPP method (called the I-NLSPP method) with

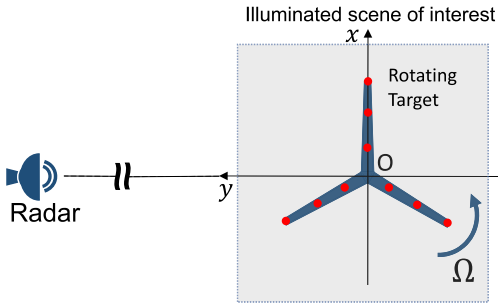

Fig. 1. The radar-target geometry for the radar imaging problem of a rotating target under consideration.

a significant performance improvement. Specifically, the proposed I-NLSPP method performs the NLSE process simultaneously over all clusters. More importantly, by doing so, the original backscattered signal received at the radar can be employed as the input of the NLSE process of the I-NLSPP method, thus no information is lost by using the imperfect reconstructed signal computed from the on-grid atoms as done in the NLSPP method [15]. Therefore, the estimates for the positions and reflectivities of the true off-grid scatterers can be obtained with higher accuracy. It is demonstrated via Monte Carlo simulations that the proposed I-NLSPP method signficantly outperforms the NLSPP method.

II. Compressive Radar Imaging of A Rotating Target

A. Problem Formulation

The problem of two-dimensional radar imaging of a rotating target with a monostatic single-frequency continuous-wave radar is depicted in Fig. 1, where the origin of the local target coordinates is placed at the rotation center of the target and the radar is located in the far field of the positive y-direction. Here, the target is modelled as a rigid ensemble of point scatterers with unknown complex-valued reflectivity coefficients.

The complex-valued energy-normalized baseband signal returned from a rotating point scatterer, after translational motion compensation, is given by [13], [14]

$$\vartheta(\boldsymbol{p},t) = A\exp\left\{\mathrm{i}\frac{4\pi}{\lambda}r\sin(\Omega t+\psi)\right\} \tag{1}$$

where $\boldsymbol{p}=[x,y]^T$ is the initial position of the scatterer, A is a normalization constant for which the signal energy over the coherent processing interval (CPI) equals to unity, λ is the radar wavelength, and $r=\sqrt{x^2+y^2}$ and $\psi=\arctan(y/x)$ are the initial radial and angular coordinates of the scatterer respectively. In this paper, Ω is the rotational speed of the target which is assumed to be constant over the CPI and known *a priori*. In practice, an accurate estimate of Ω can be readily calculated via autocorrelation methods. Note that, here and throughout the paper, i is a complex number satisfying $\mathrm{i}^2=-1$ and the superscript ^{T} denotes matrix transpose.

By performing a double integration of $\vartheta(\boldsymbol{p},t)$ in (1) over the illuminated scene of interest (i.e., over the cross-range position x and the down-range position y), the total backscattered baseband signal is given by

$$s(t) = \iint \alpha(\boldsymbol{p})\vartheta(\boldsymbol{p},t)dx\,dy \tag{2}$$

where $\alpha(\boldsymbol{p})$ is the complex-valued reflectivity coefficient at position $\boldsymbol{p}$.

By sampling $s(t)$ at times t_m $(m=1,\ldots,M)$ to form $\boldsymbol{s}=\left[\ldots,s_m,\ldots\right]^T_{m=1,\ldots,M}$ and discretizing $\alpha(\boldsymbol{p})$ over the x- and y- directions onto a grid of N points $\boldsymbol{p}_{G,n}=\left[x_{G,n},y_{G,n}\right]^T$ $(n=1,\ldots,N)$ to form $\boldsymbol{\alpha}_G=\left[\ldots,\alpha_{G,n},\ldots\right]^T_{n=1,\ldots,N}$, we obtain the following linear system of equations:

$$\boldsymbol{s}=\sum_{n=1}^{N}\alpha_{G,n}\boldsymbol{\vartheta}\left(\boldsymbol{p}_{G,n}\right)=\boldsymbol{\Phi}_G\boldsymbol{\alpha}_G \tag{3}$$

where $\boldsymbol{\Phi}_G=\left[\ldots,\boldsymbol{\vartheta}\left(\boldsymbol{p}_{G,n}\right),\ldots\right]_{n=1,\ldots,N}$ and $\boldsymbol{\vartheta}(\boldsymbol{p})=\left[\ldots,\vartheta\left(\boldsymbol{p},t_m\right),\ldots\right]^T_{m=1,\ldots,M}$. Here $\boldsymbol{\vartheta}(\boldsymbol{p})$ is the discrete version of (1) with $A=1/\sqrt{M}$. In this paper, the grid is constructed via regularly-spaced points in Cartesian coordinates with Δ denoting the grid step size on each x and y-axis. In the context of CS, the matrix $\boldsymbol{\Phi}_G$ is commonly referred to as a dictionary, and its columns $\boldsymbol{\vartheta}\left(\boldsymbol{p}_{G,n}\right)$ are referred to as atoms.

Since the backscattered radar signal is corrupted by noise in practice, (3) becomes

$$\tilde{\boldsymbol{s}}=\boldsymbol{s}(\boldsymbol{\alpha}_G)+\boldsymbol{e}=\boldsymbol{\Phi}_G\boldsymbol{\alpha}_G+\boldsymbol{e} \tag{4}$$

where $\boldsymbol{e}=\left[\ldots,e(t_m),\ldots\right]^T_{m=1,\ldots,M}$. Here, $e(t)$ is modeled as a circularly symmetric complex Gaussian random variable with variance $\sigma^2=E\{|e(t)|^2\}$.

The objective of the radar imaging problem under consideration is to reconstruct a *spatial* mapping of reflectivity distribution of the rotating target of interest by solving the inverse linear problem (4) for $\boldsymbol{\alpha}_G$ from the noisy backscattered signal $\tilde{\boldsymbol{s}}$. Since the number of pixels in the reflectivity map is often much larger than the number of received signal samples (i.e., $N\gg M$), (4) becomes underdetermined. Motivated by the sparse nature of the reflectivity vector $\boldsymbol{\alpha}_G$ due to the fact that typical targets only consist of a small number of dominant scatterers, (4) can be solved effectively within the CS framework. The sparse reconstruction algorithms available in the CS literature can be categorized into five major classes [16]: (i) greedy pursuit, (ii) convex relaxation, (iii) Bayesian framework, (iv) nonconvex optimization, and (v) brute force. Due to space limitation, we refer the readers to [1], [16], [17] for comprehensive reviews of the CS literature.

B. Technical Challenges of Conventional Sparse Reconstruction Algorithms

The linear model in (4) is only strictly valid for the idealized assumption of on-grid scatterers, i.e., the true scatterers constituting the target are located exactly on the dictionary grid nodes. However, the true scatterers are typically located in off-grid positions in practice, thus resulting in the dictionary mismatch problem.

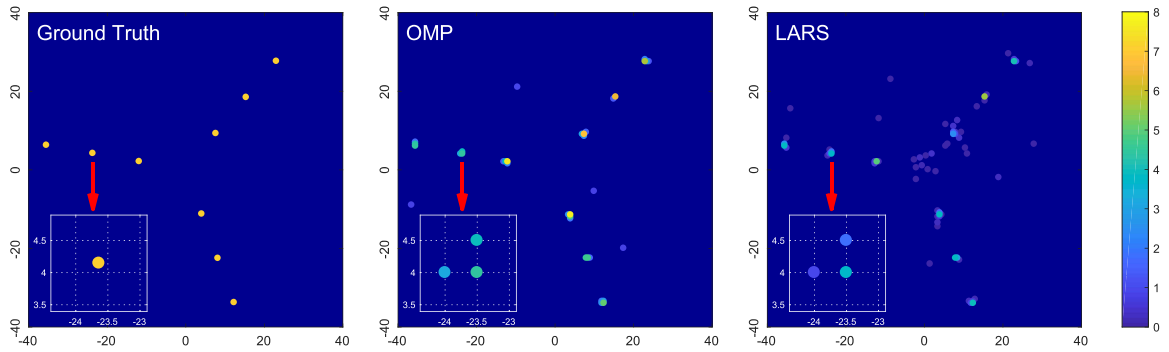

Fig. 2. Blurred images obtained by OMP and LARS for a rotating target with 9 scatterers using a dictionary with $\Delta = \lambda/6$. Note that, in all figures of this paper, the horizontal and vertical axes are the x-axis (cross-range) and y-axis (down-range), respectively, in units of centimeter, and dictionary grid nodes are located at intersections of dotted lines in zoomed-in images.

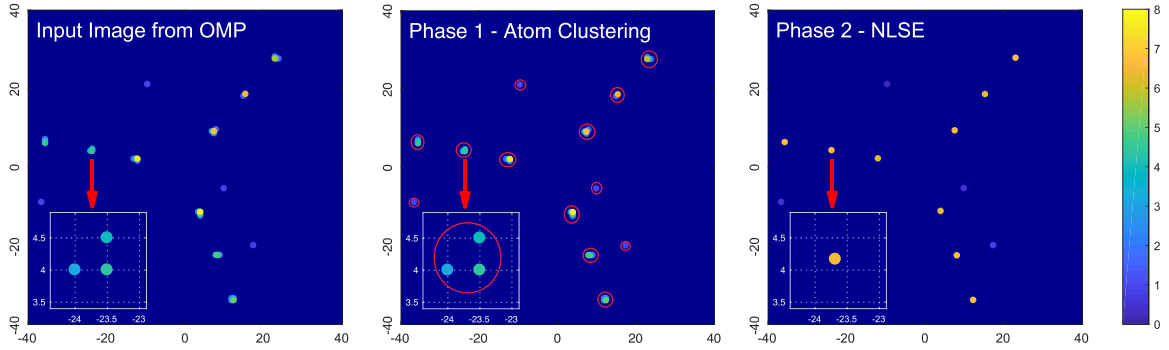

Fig. 3. Illustration of the NLSPP method [15] (the same target model as in Fig. 2).

Considering a rotating target with L dominant scatterers with reflectivity values $\alpha_{O,l}$ and off-grid positions $\boldsymbol{p}_{O,l} = \left[x_{O,l}, y_{O,l}\right]^T$ $(l = 1, \ldots, L)$, the noise-free backscattered signal vector returned from the target is given by

$$\boldsymbol{s} = \sum_{l=1}^{L} \alpha_{O,l} \boldsymbol{\vartheta}\left(\boldsymbol{p}_{O,l}\right) = \boldsymbol{\Phi}_O \boldsymbol{\alpha}_O \tag{5}$$

where $\boldsymbol{\Phi}_O = \left[\ldots, \boldsymbol{\vartheta}\left(\boldsymbol{p}_{O,l}\right), \ldots\right]_{l=1,\ldots,L}$ and $\boldsymbol{\alpha}_O = \left[\ldots, \alpha_{O,l}, \ldots\right]^T_{l=1,\ldots,L}$. Since the true scatterers are located off-grid, i.e., $\left\{\boldsymbol{p}_{O,l}\right\} \notin \left\{\boldsymbol{p}_{G,n}\right\}$, $\boldsymbol{\Phi}_O$ is not a submatrix of $\boldsymbol{\Phi}_G$ and thus $\boldsymbol{\Phi}_O \boldsymbol{\alpha}_O \neq \boldsymbol{\Phi}_G \boldsymbol{\alpha}_G$. Consequently, given a sufficiently dense dictionary grid, we only have the approximation of $\boldsymbol{s} \approx \boldsymbol{\Phi}_G \boldsymbol{\alpha}_G$ and thus

$$\tilde{\boldsymbol{s}} \approx \boldsymbol{\Phi}_G \boldsymbol{\alpha}_G + \boldsymbol{e}. \tag{6}$$

This dictionary mismatch problem results in the blurriness in the reconstructed image obtained via sparse reconstruction algorithms.

To demonstrate such a performance limitation, Fig. 2 shows the reconstructed images obtained by Orthogonal Matching Pursuit (OMP) [18], a greedy pursuit technique, and Least Angle Regression (LARS) [19], a convex relaxation technique, for a simulated target with 9 off-grid scatterers. We observe that each true scatterer induces a group of several on-grid atoms in its surrounding vicinity due to the off-grid problem. In addition, the reflectivity coefficients of these on-grid atoms calculated by OMP and LARS are much lower than the reflectivity coefficient of the true scatterer because the signal energy of the true scatterer is spread over multiple on-grid atoms. Consequently, the reconstructed images are blurred and low-contrast compared to the ground-truth image.

C. The NLSPP Method [15]

The NLSPP method, illustrated in Fig. 3, is comprised of two phases: (i) atom clustering and (ii) NLSE process. Given the on-grid atoms obtained from a sparse reconstruction algorithm, the atom clustering phase aims to partition these atoms into separate clusters, each corresponding to a true off-grid scatterer. Each cluster is then replaced by an estimated off-grid scatterer whose position and reflectivity are calculated in the NLSE process.

Note that, in addition to genuine atoms that corresponds to the true scatterers, the sparse reconstruction algorithm may obtain spurious atoms due to noise as demonstrated in Fig. 3. Such spurious atoms typically are individually isolated and will be treated as 'single-point' clusters by the atom clustering phase.

1) Atom Clustering: The NLSPP method performs atom clustering by using the K-means clustering algorithm. The K-means algorithm is one the most widely-used algorithms for clustering thanks to its simplicity and empirical success.

$$\text{Real}\left\{\alpha_{O,k}\boldsymbol{\vartheta}(\boldsymbol{p}_{O,k})\right\} = \left[\ldots, A(\text{Real}\{\alpha_{O,k}\}\cos\Phi_{O,k,m} - \text{Imag}\{\alpha_{O,k}\}\sin\Phi_{O,k,m}), \ldots\right]^T_{m=1,\ldots,M} \tag{11a}$$

$$\text{Imag}\left\{\alpha_{O,k}\boldsymbol{\vartheta}(\boldsymbol{p}_{O,k})\right\} = \left[\ldots, A(\text{Real}\{\alpha_{O,k}\}\sin\Phi_{O,k,m} + \text{Imag}\{\alpha_{O,k}\}\cos\Phi_{O,k,m}), \ldots\right]^T_{m=1,\ldots,M} \tag{11b}$$

$$\Phi_{O,k,m} = \frac{4\pi}{\lambda}(x_{O,k}\sin(\Omega t_m) + y_{O,k}\cos(\Omega t_m)). \tag{11c}$$

Let $\boldsymbol{p}_h$ $(h = 1, \ldots, H)$ denote the locations of H atoms obtained by the sparse reconstruction algorithm, the K-means algorithm aims to partition them into K clusters $\boldsymbol{C}_k$ ($k = 1, \ldots, K$) by minimizing the sum of squares of distances between the atoms and the corresponding cluster centroids [20]:

$$f(\boldsymbol{C}_1, \ldots, \boldsymbol{C}_K) = \sum_{k=1}^{K}\sum_{\boldsymbol{p}_h \in \boldsymbol{C}_k} \|\boldsymbol{p}_h - \boldsymbol{\mu}_k\|^2 \tag{7}$$

where $\boldsymbol{\mu}_k$ denotes the centroid coordinate of the cluster $\boldsymbol{C}_k$. The K-means algorithm minimizes this objective function by starting with a random partition, and iteratively reassigning each atom to its closest centroid and recomputing new cluster centroids (see, e.g. [20] for details).

Since the number of clusters K is unknown, the NLSPP method performs the K-means algorithm for various values of K. In particular, K starts with the value of 1 and increases until the radii of all clusters fall below a preset threshold. The cluster radius is defined as the distance from the centroids to the farthest atom member. The preset threshold for cluster radius should be chosen so that all appropriate atoms clustered around the true scatterers are included to form the genuine clusters associated with the true scatterers while spurious atoms are excluded from these genuine clusters. The numerical studies in [15] recommend the threshold value of $\lambda/2$.

2) NLSE process: We consider a particular cluster $\boldsymbol{C}_k$ obtained from the atom clustering phase. Let $\boldsymbol{p}_{k,u} = [x_{k,u}, y_{k,u}]^T$ and $\hat{\alpha}_{k,u}$ for $u = 1, 2, \ldots, U$ denote the positions and reflectivities coefficients of U atom members in the cluster $\boldsymbol{C}_k$. Assuming that this cluster is genuine and it corresponds to a true scatterer with position $\boldsymbol{p}_{O,k} = [x_{O,k}, y_{O,k}]^T$ and reflectivity coefficient $\alpha_{O,k}$, the summed reconstructed backscattered signal $\tilde{\boldsymbol{s}}_k$ of all the atoms in the cluster is an estimate of the true backscattered signal $\boldsymbol{s}_{O,k}$ of the scatterer:

$$\tilde{\boldsymbol{s}}_k \approx \boldsymbol{s}_{O,k} \tag{8}$$

where $\tilde{\boldsymbol{s}}_k = \sum_{u=1}^{U}\hat{\alpha}_{k,u}\boldsymbol{\vartheta}(\boldsymbol{p}_{k,u})$ and $\boldsymbol{s}_{O,k} = \alpha_{O,k}\boldsymbol{\vartheta}(\boldsymbol{p}_{O,k})$

Since $\boldsymbol{s}_{O,k}$ is the function of $\alpha_{O,k}$ and $\boldsymbol{p}_{O,k}$, the NLSE process aims to estimate $\alpha_{O,k}$ and $\boldsymbol{p}_{O,k}$ by minimizing the following least-squares criterion:

$$\underset{\{\alpha_{O,k}, \boldsymbol{p}_{O,k}\}}{\text{minimize}} \left\|\tilde{\boldsymbol{s}}_k - \alpha_{O,k}\boldsymbol{\vartheta}(\boldsymbol{p}_{O,k})\right\|_2 \tag{9}$$

which is equivalent to

$$\underset{\{\alpha_{O,k}, \boldsymbol{p}_{O,k}\}}{\text{minimize}} \left\| \begin{bmatrix}\text{Real}\{\tilde{\boldsymbol{s}}_k\}\\ \text{Imag}\{\tilde{\boldsymbol{s}}_k\}\end{bmatrix} - \begin{bmatrix}\text{Real}\left\{\alpha_{O,k}\boldsymbol{\vartheta}(\boldsymbol{p}_{O,k})\right\}\\ \text{Imag}\left\{\alpha_{O,k}\boldsymbol{\vartheta}(\boldsymbol{p}_{O,k})\right\}\end{bmatrix}\right\|_2 \tag{10}$$

where the expressions for $\text{Real}\left\{\alpha_{O,k}\boldsymbol{\vartheta}(\boldsymbol{p}_{O,k})\right\}$ and $\text{Imag}\left\{\alpha_{O,k}\boldsymbol{\vartheta}(\boldsymbol{p}_{O,k})\right\}$ are given in (11).

By letting $\tilde{\boldsymbol{z}}_k = \left[\text{Real}\{\tilde{\boldsymbol{s}}_k\}^T, \text{Imag}\{\tilde{\boldsymbol{s}}_k\}^T\right]^T$ and $\boldsymbol{z}_{O,k} = \left[\text{Real}\left\{\alpha_{O,k}\boldsymbol{\vartheta}(\boldsymbol{p}_{O,k})\right\}^T, \text{Imag}\left\{\alpha_{O,k}\boldsymbol{\vartheta}(\boldsymbol{p}_{O,k})\right\}^T\right]^T$ and writing $\boldsymbol{z}_{O,k}(\boldsymbol{\xi}_{O,k})$ as an explicit function of $\boldsymbol{\xi}_{O,k} = \left[\alpha^R_{O,k}, \alpha^I_{O,k}, x_{O,k}, y_{O,k}\right]^T$ ($\alpha^R_{O,k} = \text{Real}\{\alpha_{O,k}\}$ and $\alpha^I_{O,k} = \text{Imag}\{\alpha_{O,k}\}$), (10) becomes

$$\underset{\boldsymbol{\xi}_{O,k}}{\text{minimize}} \left\|\tilde{\boldsymbol{z}}_{O,k} - \boldsymbol{z}_{O,k}(\boldsymbol{\xi}_{O,k})\right\|_2 \tag{12}$$

which is a NLSE problem in the real-valued domain. This NLSE problem can be solved numerically via Gauss-Newton (GN) iteration [21] as

$$\begin{aligned}\hat{\boldsymbol{\xi}}_{O,k}(j+1) = \hat{\boldsymbol{\xi}}_{O,k}(j) + \left(\boldsymbol{\Gamma}^T_k(j)\boldsymbol{\Gamma}_k(j)\right)^{-1}\boldsymbol{\Gamma}^T_k(j)\\ \times\left(\tilde{\boldsymbol{z}}_k - \boldsymbol{z}_{O,k}\left(\hat{\boldsymbol{\xi}}_{O,k}(j)\right)\right)\end{aligned} \tag{13}$$

for $j = 0, 1, \ldots,$ where $\boldsymbol{\Gamma}_k(j) = \boldsymbol{\Gamma}_k\left(\hat{\boldsymbol{\xi}}_{O,k}(j)\right)$ is the Jacobian matrix of $\boldsymbol{z}_{O,k}$ with respect to $\boldsymbol{\xi}_{O,k}$ evaluated at $\boldsymbol{\xi}_{O,k} = \hat{\boldsymbol{\xi}}_{O,k}(j)$, and $\boldsymbol{z}_{O,k}\left(\hat{\boldsymbol{\xi}}_{O,k}(j)\right)$ is an estimate of $\boldsymbol{z}_{O,k}$ calculated at $\boldsymbol{\xi}_{O,k} = \hat{\boldsymbol{\xi}}_{O,k}(j)$. The Jacobian matrix $\boldsymbol{\Gamma}_k\left(\boldsymbol{\xi}_{O,k}\right)$ is straightforward to derive and its expression can be found in [15].

The GN algorithm (13) is initialized based on the signal energy of $\tilde{\boldsymbol{s}}_k$ and the energy-weighted center of the cluster $\boldsymbol{C}_k$:

$$\hat{\boldsymbol{\xi}}_{O,k}(0) = \left[\hat{\alpha}^R_{O,k}(0), \hat{\alpha}^I_{O,k}(0), \hat{x}_{O,k}(0), \hat{y}_{O,k}(0)\right]^T \tag{14}$$

where $\hat{\alpha}^R_{O,k}(0) = \hat{\alpha}^I_{O,k}(0) = \|\tilde{\boldsymbol{s}}_k\|_2/\sqrt{2}$, $\hat{x}_{O,k}(0) = \dfrac{\sum_{u=1}^{U}|\hat{\alpha}_{k,u}|^2 x_{k,u}}{\sum_{u=1}^{U}|\hat{\alpha}_{k,u}|^2}$, and $\hat{y}_{O,k}(0) = \dfrac{\sum_{u=1}^{U}|\hat{\alpha}_{k,u}|^2 y_{k,u}}{\sum_{u=1}^{U}|\hat{\alpha}_{k,u}|^2}$.

Each cluster $\boldsymbol{C}_k$ is now replaced by a single estimated off-grid scatterer with position $\hat{\boldsymbol{p}}^{\text{GN}}_{O,k}$ and reflectivity coefficient $\hat{\alpha}^{\text{GN}}_{O,k}$ extracted from the solution $\hat{\boldsymbol{\xi}}_{O,k}(j_{\text{final}})$ of the GN algorithm (13). Note that, for the case of a single-point cluster which contains only one atom (i.e., $U = 1$), the GN solution is simply the position and reflectivity coefficient of this atom: $\hat{\boldsymbol{p}}^{\text{GN}}_{O,k} = \boldsymbol{p}_{k,1}$ and $\hat{\alpha}^{\text{GN}}_{O,k} = \hat{\alpha}_{k,1}$.

Finally, a linear least-squares estimation is performed over these estimated scatterers to re-calculate their reflectivity values based on the total backscattered signal $\tilde{\boldsymbol{s}}$ to further improve the accuracy of reflectivity estimates:

$$[\hat{\hat{\alpha}}_{O,1}, \ldots, \hat{\hat{\alpha}}_{O,K}]^T = \left(\boldsymbol{\Psi}^{\mathcal{H}}\boldsymbol{\Psi}\right)^{-1}\boldsymbol{\Psi}^{\mathcal{H}}\tilde{\boldsymbol{s}} \tag{15}$$

where $\boldsymbol{\Psi} = \left[\ldots, \boldsymbol{\vartheta}\left(\hat{\boldsymbol{p}}^{\text{GN}}_{O,k}\right), \ldots\right]_{k=1,\ldots,K}$ and the subscript $^{\mathcal{H}}$ denotes the Hermitian transpose operation.

III. The Proposed I-NLSPP Method

The disadvantage of the NLSPP method summarized in Section II-C that it performs the NLSE procedure for each cluster $\boldsymbol{C}_k$ individually using the summed reconstructed backscattered signal $\tilde{\boldsymbol{s}}_k$ computed from the atoms within the cluster. However, the reconstructed signal $\tilde{\boldsymbol{s}}_k$ is only a reasonable but not highly accurate estimate of the actual backscattered signal $\boldsymbol{s}_{O,k}$ of the true scatterer due to the mismatch between the scatterer position and the dictionary grid nodes. Consequently, this limits the accuracy of the NLSE estimates and thus the overall performance of the NLSPP method.

To overcome such a problem, the proposed I-NLSPP method aims to perform the NLSE process simultaneously over all clusters to estimate the positions and reflectivities of all scatterers in a joint manner. Most importantly, this allows the I-NLSPP method to employ the original backscattered signal $\tilde{\boldsymbol{s}}$ as the input to the joint NLSE process. Note that, although the original signal $\tilde{\boldsymbol{s}}$ is a noisy signal due to the noise in radar hardware, it is not affected by the off-grid mismatch problem which is the main cause of the limitation in the accuracy of the reconstructed signal $\tilde{\boldsymbol{s}}_k$ (that, in turn, upsets the performance of the NLSPP method). As a result, the I-NLSPP can estimate the positions and reflectivities of the off-grid scatterers with higher accuracy. Note that the atom clustering step remains the same in the I-NLSPP method.

The main idea behind the proposed joint NLSE process is to simultaneously estimate $\{\alpha_{O,1},\ldots,\alpha_{O,K}\}$ and $\{\boldsymbol{p}_{O,1},\ldots,\boldsymbol{p}_{O,K}\}$ using the summed version of the least-squares criterion in (9) over $k=1,\ldots,K$ as

$$\underset{\substack{\alpha_{O,1},\ldots,\alpha_{O,K}\\ \boldsymbol{p}_{O,1},\ldots,\boldsymbol{p}_{O,K}}}{\text{minimize}} \left\| \sum_{k=1}^{K} \left(\tilde{\boldsymbol{s}}_k - \alpha_{O,k}\boldsymbol{\vartheta}(\boldsymbol{p}_{O,k}) \right) \right\|_2 . \tag{16}$$

Since $\sum_{k=1}^{K}\tilde{\boldsymbol{s}}_k$ is the reconstructed version of the original backscattered signal $\tilde{\boldsymbol{s}}$, it is desirable to replace $\sum_{k=1}^{K}\tilde{\boldsymbol{s}}_k$ with $\tilde{\boldsymbol{s}}$ in (16), thus leading to

$$\underset{\substack{\alpha_{O,1},\ldots,\alpha_{O,K}\\ \boldsymbol{p}_{O,1},\ldots,\boldsymbol{p}_{O,K}}}{\text{minimize}} \left\| \tilde{\boldsymbol{s}} - \sum_{k=1}^{K} \alpha_{O,k}\boldsymbol{\vartheta}(\boldsymbol{p}_{O,k}) \right\|_2 . \tag{17}$$

This minimization is equivalent to

$$\underset{\substack{\alpha_{O,1},\ldots,\alpha_{O,K}\\ \boldsymbol{p}_{O,1},\ldots,\boldsymbol{p}_{O,K}}}{\text{minimize}} \left\| \begin{bmatrix} \text{Real}\{\tilde{\boldsymbol{s}}\} \\ \text{Imag}\{\tilde{\boldsymbol{s}}\} \end{bmatrix} - \sum_{k=1}^{K} \begin{bmatrix} \text{Real}\left\{\alpha_{O,k}\boldsymbol{\vartheta}(\boldsymbol{p}_{O,k})\right\} \\ \text{Imag}\left\{\alpha_{O,k}\boldsymbol{\vartheta}(\boldsymbol{p}_{O,k})\right\} \end{bmatrix} \right\|_2 \tag{18}$$

or

$$\underset{\boldsymbol{\xi}_O}{\text{minimize}} \left\| \tilde{\boldsymbol{z}} - \boldsymbol{z}_O(\boldsymbol{\xi}_O) \right\|_2 \tag{19}$$

where we define $\tilde{\boldsymbol{z}} = \left[\text{Real}\{\tilde{\boldsymbol{s}}\}^T, \text{Imag}\{\tilde{\boldsymbol{s}}\}^T\right]^T$ and $\boldsymbol{z} = \sum_{k=1}^{K}\left[\text{Real}\left\{\alpha_{O,k}\boldsymbol{\vartheta}(\boldsymbol{p}_{O,k})\right\}^T, \text{Imag}\left\{\alpha_{O,k}\boldsymbol{\vartheta}(\boldsymbol{p}_{O,k})\right\}^T\right]^T$ and $\boldsymbol{\xi}_O = \left[\ldots, \boldsymbol{\xi}_{O,k}^T, \ldots\right]_{k=1,\ldots,i}^T$. The GN solution for the minimization (19) is

$$\hat{\boldsymbol{\xi}}_O(j+1) = \hat{\boldsymbol{\xi}}_O(j) + \left(\boldsymbol{\Gamma}^T(j)\boldsymbol{\Gamma}(j)\right)^{-1}\boldsymbol{\Gamma}^T(j)\left(\tilde{\boldsymbol{z}} - \boldsymbol{z}_O\left(\hat{\boldsymbol{\xi}}_O(j)\right)\right) \tag{20}$$

for $j=0,1,\ldots$, where $\boldsymbol{\Gamma}(j) = [\ldots, \boldsymbol{\Gamma}_k(j), \ldots]_{k=1,\ldots,K}^T$ is the Jacobian matrix and the initial value is given by $\hat{\boldsymbol{\xi}}_O(0) = \left[\ldots, \hat{\boldsymbol{\xi}}_{O,k}^T(0), \ldots\right]_{k=1,\ldots,K}^T$. Details of $\boldsymbol{\Gamma}_k(j)$ and $\hat{\boldsymbol{\xi}}_{O,k}(0)$ can be found in Section II-C. The GN algorithm is halted after a preset number of iterations or based on the norm of the relative difference between two consecutive estimates.

It should be noted that the number of clusters is typically larger than the number of true scatterers (i.e., $K > L$) because the sparse reconstruction algorithm also collects spurious atoms due to noise. Therefore, the positions and reflectivities of the true scatterers are estimated along with those of the spurious atoms in the joint NLSE process. Although the I-NLSPP method (as with the NLSPP method) does not directly eliminate the spurious atoms, the estimated reflectivity coefficients of spurious atoms are significantly reduced by the NLSE process.

IV. Numerical Results

We consider a synthetic target with 12 scatterers rotating at $\Omega = 31.4159$ rad/sec as shown in Fig. 4. The radial distances of the scatterers from the rotational center $[0,0]^T$ are $0.12, 0.24, 0.36$ and 0.48 m and their angles with respect to the x-axis are -68°, 52° and 172°. In the simulation, the following parameter settings are used: $\lambda = 0.03$ m, $M = 960$, $\Delta = \lambda/7$, and the sampling frequency $f_s = 6$ kHz. The OMP algorithm is halted when the signal residual attains the noise level. The GN algorithms of the NLSPP and I-NLSPP methods are terminated after 20 iterations.

Fig. 4 compares the reconstructed images obtained by the OMP, NLSPP and I-NLSPP methods for signal-to-noise ratio $\text{SNR} = 10$ dB. Here, the OMP image is used as the input of the NLSPP and I-NLSPP methods. In contrast to the blurred OMP image, both the NLSPP and I-NLSPP methods produce sharp and correct-intensive images that are almost identical to the true image. We also observe in the zoomed-in images that the proposed I-NLSPP method results in a more accurate estimated scatterer (i.e., its position and reflectivity color are closer to the true values) than the NLSPP method. To further support this observation, we evaluate the root-mean-squared-error (RMSE) for the scatterer position and reflectivity estimates obtained by the NLSPP and I-NLSPP methods via 500 Monte Carlo simulation runs. The Cramér-Rao lower bounds are also calculated and their square root (RCRLB) values are used as theoretical benchmarks for RMSE performance. Fig. 5 compares the RMSE performance of the NLSPP and I-NLSPP methods for various SNR values, where the I-NLSPP method exhibits RMSE performance much closer to the RCRLB than the NLSPP method. This thus demonstrates the performance superiority of the I-NLSPP method over the NLSPP method in terms of estimating the unknown positions and reflectivities of the true scatterers. We also observe that the I-NLSSP and NLSPP methods have similar runtimes.

V. Conclusion

The paper has proposed a new improvement of the NLSPP method, namely the I-NLSPP method, to resolve the blurring

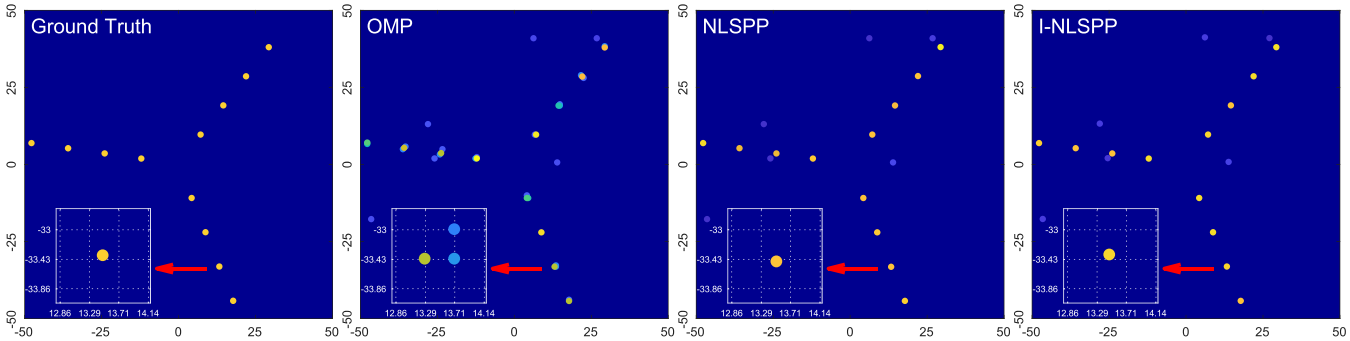

Fig. 4. Comparison of reconstructed images obtained by the OMP, NLSPP and I-NLSPP methods (the same colorbar scale as Fig. 2 is used).

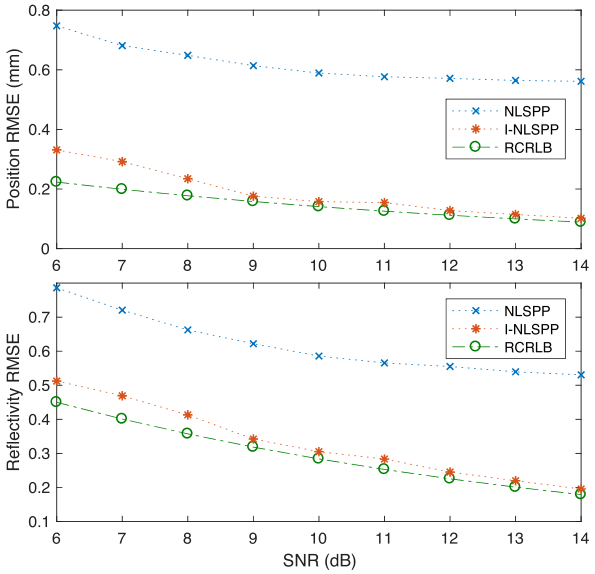

Fig. 5. RMSE comparison between the NLSPP and I-NLSPP methods.

problem existing in the reconstructed images of a rotating target obtained by conventional sparse reconstruction algorithms. In contrast to the NLSPP method, the proposed I-NLSPP method performs the NLSE process jointly over all atom clusters using the original backscattered signal, thus resulting in more accurate estimates of the positions and reflecitivies of the true off-grid scatterers. Numerical simulations were presented to corroborate the advantage of the proposed I-NLSPP method over the NLSPP method, where the I-NLSPP method is observed to attain a RMSE performance much closer to the RCRLB than the NLSPP method.

REFERENCES

[1] L. C. Potter, E. Ertin, J. T. Parker, and M. Cetin, "Sparsity and compressed sensing in radar imaging," *Proc. IEEE*, vol. 98, no. 6, pp. 1006–1020, Jun. 2010.

[2] R. Baraniuk and P. Steeghs, "Compressive radar imaging," in *IEEE Radar Conf.*, Boston, MA, USA, April 2007, pp. 128–133.

[3] O. Teke, A. C. Gurbuz, and O. Arikan, "A robust compressive sensing based technique for reconstruction of sparse radar scenes," *Digit. Signal Process.*, vol. 27, pp. 23–32, 2014.

[4] M. Cetin and W. C. Karl, "Feature-enhanced synthetic aperture radar image formation based on nonquadratic regularization," *IEEE Trans. Image Process.*, vol. 10, no. 4, pp. 623–631, Apr. 2001.

[5] M. Cetin, W. C. Karl, and A. S. Willsky, "Feature-preserving regularization method for complex-valued inverse problems with application to coherent imaging," *Opt. Eng.*, vol. 45, no. 1, pp. 1–11, 2006.

[6] N. Ramakrishnan, E. Ertin, and R. L. Moses, "Enhancement of coupled multichannel images using sparsity constraints," *IEEE Trans. Image Process.*, vol. 19, no. 8, pp. 2115–2126, Aug. 2010.

[7] K. R. Varshney, M. Cetin, J. W. Fisher, and A. S. Willsky, "Sparse representation in structured dictionaries with application to synthetic aperture radar," *IEEE Trans. Signal Process.*, vol. 56, no. 8, pp. 3548–3561, Aug. 2008.

[8] I. Stojanovic and W. C. Karl, "Imaging of moving targets with multi-static SAR using an overcomplete dictionary," *IEEE J. Sel. Topics Signal Process.*, vol. 4, no. 1, pp. 164–176, Feb. 2010.

[9] S. Kodituwakku, R. Melino, P. E. Berry, and H. T. Tran, "Tilted-wire scatterer model for narrowband radar imaging of rotating blades," *IET Radar, Sonar Navig.*, vol. 11, no. 4, pp. 640–645, 2017.

[10] N. H. Nguyen, H. T. Tran, K. Dogancay, and R. Melino, "A review of sparsity-based methods for analysing radar returns from helicopter rotor blades," DST Group, DST-Group-TR-3292, Tech. Rep., Sep. 2016.

[11] N. H. Nguyen, K. Dogancay, P. Berry, and H. T. Tran, "Convex relaxation methods: A review and application to sparse radar imaging of rotating targets," DST Group, DST-Group-RR-0444, Tech. Rep., Sep. 2017.

[12] R. Melino, S. Kodituwakku, and H. T. Tran, "Orthogonal matching pursuit and matched filter techniques for the imaging of rotating blades," in *Proc. IEEE Radar Conf.*, Oct. 2015, pp. 1–6.

[13] V. C. Chen, *The Micro-Doppler Effect in Radar*. Norwood: Artech House, 2011.

[14] V. C. Chen, F. Li, S. S. Ho, and H. Wechsler, "Micro-Doppler effect in radar: phenomenon, model, and simulation study," *IEEE Trans. Aerosp. Electron. Syst.*, vol. 42, no. 1, pp. 2–21, Jan. 2006.

[15] N. H. Nguyen, K. Dogancay, H. T. Tran, and P. Berry, "An image focusing method for sparsity-driven radar imaging of rotating targets," *Sensors*, vol. 18, no. 6, pp. 1–20, 2018.

[16] J. A. Tropp and S. J. Wright, "Computational methods for sparse solution of linear inverse problems," *Proc. IEEE*, vol. 98, no. 6, pp. 948–958, Jun. 2010.

[17] Y. C. Eldar and G. Kutyniok, Eds., *Compressed Sensing: Theory and Applications*. New York: Cambridge University Press, 2012.

[18] Y. C. Pati, R. Rezaiifar, and P. S. Krishnaprasad, "Orthogonal matching pursuit: recursive function approximation with applications to wavelet decomposition," in *Proc. 27th Asilomar Conf. Signals, Syst., Comput.*, vol. 1, Nov. 1993, pp. 40–44.

[19] B. Efron, T. Hastie, I. Johnstone, and R. Tibshirani, "Least angle regression," *Ann. Statist.*, vol. 32, no. 2, pp. 407–499, Apr. 2004.

[20] P. Drineas, A. Frieze, R. Kannan, S. Vempala, and V. Vinay, "Clustering large graphs via the singular value decomposition," *Machine Learn.*, vol. 56, no. 1, pp. 9–33, 2004.

[21] L. Ljung and T. Soderstrom, *Theory and Practice of Recursive Identification*. Cambridge, MA: MIT Press, 1983.